AGU100 ADVANCING EARTH AND SPACE SCIENCE

Geophysical Research Letters

RESEARCH LETTER
10.1029/2018GL078882

Key Points:
- A novel partial coupling method isolates atmosphere- and ocean-forced components of Atlantic multidecadal variability (AMV)
- The atmosphere-forced AMV component is weak, while the ocean-forced AMV component is strong and imprinted on the surface heat fluxes
- The weak multidecadal power of the fully coupled AMV is due to damping of the ocean-forced variability by strong air-sea coupling

Supporting Information:
- Supporting Information S1

Correspondence to:
O. A. Garuba,
Oluwayemi.Garuba@pnnl.gov

Citation:
Garuba, O. A., Lu, J., Singh, H. A., Liu, F., & Rasch, P. (2018). On the relative roles of the atmosphere and ocean in the Atlantic multidecadal variability. *Geophysical Research Letters*, *45*, 9186–9196. https://doi.org/10.1029/2018GL078882

Received 3 JUN 2018
Accepted 1 AUG 2018
Accepted article online 8 AUG 2018
Published online 12 SEP 2018

On the Relative Roles of the Atmosphere and Ocean in the Atlantic Multidecadal Variability

Oluwayemi A. Garuba[1], Jian Lu[1], Hansi A. Singh[1], Fukai Liu[2], and Phil Rasch[1]

[1]Pacific Northwest National Laboratory, Richland, WA, USA, [2]Ocean University of China, Qingdao, China

Abstract The relative roles of the ocean and atmosphere in driving the Atlantic multidecadal variability (AMV) are investigated by isolating anomalous sea surface temperature (SST) components forced by anomalous surface heat fluxes and ocean dynamics in fully and partially coupled simulations. The impact of the ocean dynamics-forced SST on air-sea interaction is disabled in the partially coupled simulation in order to isolate the atmosphere-forced variability. The atmosphere-forced AMV component shows weak but significant variability on interdecadal timescales (10- to 30-year periods), while the ocean-forced component exhibits a strong multidecadal variability (25- to 50-year periods). When coupled to the atmosphere, this ocean-forced variability weakens and is imprinted on the coupled surface heat fluxes that further act to damp the ocean-forced SST variability, causing a much weaker fully coupled AMV. Our results suggest that the AMV is largely driven by ocean circulation variability, but its power is also affected by the strength of air-sea coupling.

Plain Language Summary The mechanism of the Atlantic multidecadal variability (AMV) has recently been debated. We investigate the relative roles of the ocean and atmosphere in this variability by applying an ocean temperature decomposition and partial coupling method to isolate the components of the AMV driven by the atmosphere and the ocean in a fully coupled model. We show that the ocean drives stronger multidecadal variability (greater than 30 years), while the atmosphere drives weaker variability up to interdecadal timescales (10–30 years). Surface interactions between the atmosphere and ocean decrease the ocean-driven variability, as surface heat fluxes act to damp the ocean anomalies. Our results imply that the strength of the surface coupling in global climate models might be one of the reasons why they simulate weaker AMV compared to what is found in observations.

1. Introduction

Observations and fully coupled models show that North Atlantic sea surface temperatures (SSTs) exhibit decadal to multidecadal variability, known as the Atlantic multidecadal variability (AMV; Frankcombe et al., 2010; Kushnir, 1994; Singh et al., 2018; Zhang & Wang, 2013). However, the relative roles of the atmosphere and ocean in driving this variability remains uncertain. The notion of an atmosphere-forced AMV has been proposed based on the similarities between the spectra and predictable components of the AMV in slab ocean models without an interactive ocean circulation and those of fully coupled models with interactive ocean dynamics (Cane et al., 2017; Clement et al., 2015; Srivastava & DelSole, 2017). On the other hand, several other studies have demonstrated a dominant role for the ocean in the AMV, which is often attributed to the slow variation of the Atlantic meridional overturning circulation (Delworth & Greatbatch, 2000; Gulev et al., 2013; Knight et al., 2005; Msadek & Frankignoul, 2009; O'Reilly et al., 2016; Zhang & Wang, 2013; Zhang, 2017).

The conceptual model for ocean mixed layer temperature can be used to discuss and evaluate the relative roles of the atmosphere and ocean (Barsugli & Battisti, 1998; Frankignoul, 1985; Frankignoul et al., 2002; Goodman & Marshall, 1999; Zhang, 2017):

$$\rho c_p h \frac{\partial T'}{\partial t} = Q'_{\text{net}} + Q'_O = q'_A - \lambda_A T' + q'_O - \lambda_O T'. \quad (1)$$

Equation (1) implies that the ocean mixed layer temperature change $\frac{\partial T'}{\partial t}$ is due to the balance between the net anomalous surface heat fluxes (Q'_{net}, decomposed into an atmospheric forcing [q'_A] and the surface damping of T', $\lambda_A T'$) and ocean heat convergence (Q'_O consisting of an oceanic forcing [q'_O] and the ocean damping of

T' $\lambda_O T'$). λ_A and λ_O are the surface and ocean damping rates. λ_A, λ_O, and Q'_O are often diagnosed from fully coupled models and observations. The correlation between the spatially averaged T' (AMV index) and Q'_{net} or Q'_O has been used to infer the relative roles of the atmospheric and oceanic forcings (q'_A and q'_O). Using the convention that surface heat fluxes into the ocean are positive, at low frequencies, $-Q'_{\text{net}}$ shows a positive correlation with T' at positive lead times, while the $\{-Q'_O, T'\}$ correlation is negative in fully coupled models and observations, indicating an ocean-forced variability damped by surface heat fluxes. On the other hand, slab models show a negative $\{-Q'_{\text{net}}, T'\}$ correlation, indicating a different mechanism (Clement et al., 2015; Gulev et al., 2013; O'Reilly et al., 2016; Zhang et al., 2016).

However, the inferences based on the correlation of Q'_{net} or Q'_O with T' have been debated. In a stochastic model based on (1), in which q'_A and Q'_O can be prescribed, O'Reilly et al. (2016) found a negative $\{-Q'_{\text{net}}, T'\}$ correlation when Q'_{net} leads, by prescribing q'_A as white noise and $Q'_O = 0$ (note that prescribing Q'_O makes it independent of T' and implies $\lambda_O = 0$ or $Q'_O = q'_O$). When Q'_O was prescribed as a periodic function of time, they found a positive $\{-Q'_{\text{net}}, T'\}$ correlation, arguing that a periodic ocean convergence is necessary for the positive $\{-Q'_{\text{net}}, T'\}$ correlation. However, Clement et al. (2016) and Cane et al. (2017) also found the positive $\{-Q'_{\text{net}}, T'\}$ correlation, when both q'_A and Q'_O were prescribed as white noise, suggesting that a periodic ocean heat convergence is not necessarily the reason for the positive $\{-Q'_{\text{net}}, T'\}$ correlation.

Zhang (2017) later showed that inferences on the relative roles of q'_A and q'_O can be made from the $\{Q'_O, T'\}$ or $\{Q'_{\text{net}}, T'\}$ correlation, if the relative magnitudes of λ_O and λ_A are known. Given that $\lambda_O \approx \lambda_A$ over the midlatitude oceans, the correlation $\{Q'_O, T'\}$ can only be positive if $q'_O \gg q'_A$. The review above highlights the importance of disentangling the roles of atmosphere and ocean in fully coupled climate phenomena. As highlighted above the surface heat flux, Q'_{net} and ocean heat convergence, Q'_O, both depend on T' through their respective damping terms and therefore include components caused by both atmospheric and oceanic forcings and do not isolate atmosphere- and ocean-forced components of T'.

In this study we explicitly isolate the atmosphere- and ocean-forced components of T', in order to quantify their relative roles and to validate the mathematical formula derived from the conceptual model by Zhang (2017). First, we decompose ocean temperature variability into parts forced by the anomalous surface heat fluxes and ocean circulation using the passive tracer decomposition approach described in Banks and Gregory (2006), Xie and Vallis (2012), Bouttes et al. (2014), Marshall et al. (2015), Garuba and Klinger (2016), and Gregory et al. (2016), except here we decompose ocean temperature anomalies due to internal variability rather than those due to CO_2 forcing as in these earlier studies. Further using the partial coupling approach introduced in Garuba et al. (2018), we isolate the atmosphere-forced component of the surface heat fluxes by preventing the ocean-forced SST component from interacting with the atmosphere. Using the spectra of the AMV index and its components, and their phase relationship and correlation with surface turbulent fluxes in the partially and fully coupled simulations, we show how the interactions between the atmosphere- and ocean-forced components generate fully coupled AMV variability.

2. Methods

2.1. Model and Experimental Design

We use the coupled and slab ocean configurations of the community Earth System Model version1.1 (CESM 1.1 and CESM-SOM). The fully coupled CESM consists of the following active components: Community Atmospheric Model version 5 (CAM5; Neale et al., 2010), Parallel Ocean Program version 2 (POP2; Danabasoglu et al., 2012), Community Land Model version 4 (CLM4; Oleson et al., 2010), and the Community Ice CodE (CICE; Hunke et al., 2010). In the CESM-SOM, the ocean model POP is replaced by a slab ocean model with a spatially varying mixed layer depth (SOM; see ; Bitz et al., 2012). CAM5 and CLM4 use a 2.5° × 1.9° horizontal resolution, with 30 vertical levels in CAM5. CICE, POP, and SOM run on a nominally 1° resolution, displaced-pole grid (with the north pole singularity centered over Greenland); POP has 61 vertical levels.

Two coupled simulations (fully coupled and partially coupled; details in sections 2.2 and 2.3) and one slab simulation, each 200 years long, were performed with preindustrial radiative forcing.

2.2. Fully Coupled Decomposition

We perform a fully coupled simulation in which the ocean temperature variability anomalies (i.e., the departure from the monthly climatology) are decomposed with two passive tracers introduced in the simulation. The monthly climatology of the ocean temperature and surface heat fluxes are needed to define and track

the ocean temperature variability anomalies; these are derived from an existing control simulation that a new fully coupled simulation replicates.

The decomposition briefly described here is based on the evolution equation for total ocean temperature:

$$\frac{\partial T}{\partial t} = Q_{\text{net}} - \vec{v} \cdot \nabla T \tag{2}$$

All variables in (2) include the monthly climatological means that will be denoted by the overbar and the variability anomalies denoted by primes (e.g., $T = \bar{T} + T'$); T and $\vec{v}$ are three-dimensional total ocean temperature and circulation (all ocean transport processes) fields, respectively; Q_{net} is the net surface heat flux including the radiative and turbulent components, and $\vec{v} \cdot \nabla T$ is the ocean heat divergence due to the ocean circulation $\vec{v}$. Removing the climatological temperature evolution equation (i.e., $\frac{\partial \bar{T}}{\partial t} = \bar{Q}_{\text{net}} - \bar{\vec{v}} \cdot \nabla \bar{T}$) from (2) gives

$$\frac{\partial T'}{\partial t} = Q'_{\text{net}} - \vec{v}' \cdot \nabla \bar{T} - \vec{v} \cdot \nabla T'. \tag{3}$$

Equation (3) indicates ocean temperature variability is caused by the variability of the surface heat fluxes, and that of the ocean circulation, through the redistribution of the reservoir or climatological ocean temperature gradients. Thus, we can partition equation (3) into two parts based on these forcings:

$$\frac{\partial T'_{AF}}{\partial t} = Q'_{\text{net}} - \vec{v} \cdot \nabla T'_{AF}, \tag{4}$$

$$\frac{\partial T'_{RF}}{\partial t} = -\vec{v}' \cdot \nabla \bar{T} - \vec{v} \cdot \nabla T'_{RF}, \tag{5}$$

such that equation (3) is (4) + (5), and $T' = T'_{AF} + T'_{RF}$. We refer to T'_{AF} and T'_{RF} as the *surface-forced* and *dynamics-forced* (or *redistributive*) temperature anomaly components, respectively. The subscript F in T'_{AF} and T'_{RF} denotes fully coupled temperature components.

To obtain T'_{AF} and T'_{RF}, we implement two temperature-like passive tracers (P_A and P_R) in the fully coupled simulation, as introduced in Banks and Gregory (2006) and Xie and Vallis (2012). The passive tracer P_A tracks the propagation of the temperature anomaly due to the surface heat flux anomalies from the initialization of the simulation. P_A is chosen to be 0 at initialization and forced with the interannual surface heat flux anomalies (derived by subtracting the monthly climatological surface heat fluxes from the interannually varying fully coupled surface heat fluxes). By definition P_A satisfies ((4); see supporting information S1), so that $T'_{AF} = P_A$. The second tracer, P_R, tracks the evolution of the climatological temperature ($\bar{T}$) in the simulation. Accordingly, at initialization, P_R is chosen to be $\bar{T}$, and like $\bar{T}$, forced by repeating the monthly climatological surface fluxes annually, so that $\bar{P}_R = \bar{T}$. However, because $\bar{P}$ is subject to the advection by an interannually varying circulation, it departs from $\bar{T}$ with time. It can be shown that $T'_{RF} = P_R - \bar{T}$ (see supporting information S1 or Xie & Vallis, 2012).

Relating equation (3) to the conceptual model in (1), shows that the decomposition described above only partly serves the purpose of this study, which is to isolate atmosphere-forced and ocean-forced variability components. Q'_{net} is equivalent in both equations, including atmospheric forcing (q'_A) and surface damping terms ($\lambda_A T'$); the ocean heat convergence term (Q'_O) in (1), including both oceanic forcing (q'_O) and damping terms ($\lambda_O T'$) is equivalent to $-\vec{v}' \cdot \nabla \bar{T} - \vec{v} \cdot \nabla T'$ in (3). q'_O corresponds to $-\vec{v}' \cdot \nabla \bar{T}$, as it is the forcing term due to the ocean circulation anomaly, while $\lambda_O T'$ corresponds to $-\vec{v} \cdot \nabla T'$, since it represents the oceanic removal or addition of temperature anomalies by ocean transport processes. In the midlatitude regions λ_A is shown to be large and could greatly influence the atmosphere, while λ_O is shown to be dominated by the vertical entrainment of temperature anomalies from subsurface waters in subpolar regions (Frankignoul, 1985; Frankignoul et al., 2002; Goodman & Marshall, 1999).

Therefore, T'_{RF}, the dynamics-forced component in (5) isolates the ocean-forced temperature anomaly in the fully coupled system, because it is forced only by the oceanic forcing, $\vec{v}' \cdot \nabla \bar{T}$, and excludes the atmosphere-forced component. However, T'_{AF}, the surface-forced component in (4) does not isolate the atmosphere-forced component because it is forced by Q'_{net} (which depends on both the atmospheric forcing and T' and T' includes an ocean-forced component). Note that both anomaly components are subjects to the

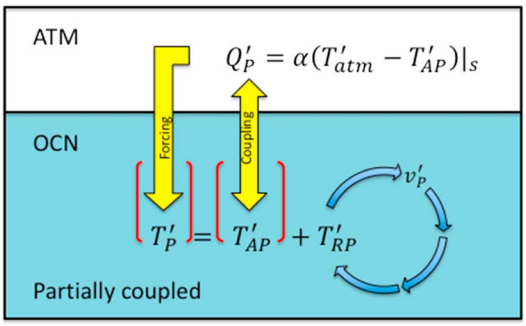

Figure 1. Schematic of the partial coupling method (adapted from ; Garuba et al., 2018)

oceanic transport or damping (i.e., $\vec{v} \cdot \nabla T'_{AF}$ and $\vec{v} \cdot \nabla T'_{RF}$); however, these damping terms are not part of the forcing for either T'_{AF} or T'_{RF}.

2.3. Partially Coupled Decomposition

In order to isolate the atmosphere-forced temperature variability, it is necessary to remove the ocean-forced SST impact from the anomalous surface heat fluxes. For this we use a partial coupling method introduced in Garuba et al. (2018). A second simulation is performed with similar model configuration and climatology as the fully coupled one, but with the anomalous surface fluxes modified using one of the tracers, such that only the variability is different between the two simulations. As in the fully coupled simulation, tracers P_A and P_R are again introduced in the partially coupled simulation, to isolate the surface-forced (T'_{AP}) and dynamics-forced (T'_{RP}) components of the ocean temperature variability anomalies (T'_P; $T'_P = T'_{AP} + T'_{RP}$; subscript P here denotes partially coupled variables).

Unlike the fully coupled simulation, the atmosphere in the partially coupled simulation is not coupled to the total temperature (i.e., $\bar{T} + T'_{AP} + T'_{RP}$); instead, it is coupled only to the surface-forced component of the temperature anomaly (i.e., $\bar{T} + T'_{AP}$), thereby removing the impact of the ocean-forced component from surface heat flux variability (described schematically in Figure 1). As a result, the partially coupled anomalous surface heat fluxes (Q'_P) depend only on atmospheric forcing and the passive ocean temperature response it causes (i.e., $q'_A - \lambda_A T'_{AP}$). The partially coupled surface-forced temperature anomaly thus isolates the atmosphere-forced variability component. The partially coupled surface-forced and dynamics-forced temperature anomalies also satisfy the following equations:

$$\frac{\partial T'_{AP}}{\partial t} = Q'_P - \vec{v} \cdot \nabla T'_{AP}, \tag{6}$$

$$\frac{\partial T'_{RP}}{\partial t} = -\vec{v}'_P \cdot \nabla \bar{T} - \vec{v} \cdot \nabla T'_{RP}. \tag{7}$$

Like its fully coupled analog, the partially coupled dynamics-forced component (T'_{RP}) is caused by ocean circulation alone (compare [5] and [7]). However, the partially coupled ocean circulation variability is different from the fully coupled one ($\vec{v}'_P \neq \vec{v}'$), because the partially coupled circulation feels atmosphere-induced surface fluxes only, while the fully coupled circulation feels both atmosphere- and ocean-induced surface fluxes. Therefore, comparing the surface-forced and dynamics-forced temperature components in the partially and fully coupled simulations reveals how coupling between the dynamic ocean response and the atmosphere impacts both surface fluxes and ocean dynamics itself; we hereafter refer to these interactions as the *ocean feedback*.

The partially coupled simulation can, in a sense, serve the same function as a slab model, which is to remove the ocean dynamical feedback in a fully coupled simulation. Therefore, it does not represent a realistic ocean but rather an ocean subject to an additional constraint, namely, that the heat fluxes are not sensitive to internal ocean variability. It is a weaker constraint than the slab because the ocean dynamics do vary, and the partially coupled surface-forced SST component, unlike the slab SSTs, includes the damping effect of ocean advective, diffusive, or mixing processes ($\vec{v} \cdot \nabla T'_{AP}$ in [6]). This lack of realistic ocean damping is one major limitation of slab simulations (Zhang, 2017). The partially coupled simulation also includes the uncoupled ocean-forced temperature component, T'_{RP}, which shows the variability the ocean induces by itself.

3. Results

3.1. AMV Components Pattern and Spectra

First, we consider the indices and pattern of the AMV and its surface-forced (AMV-SF) and ocean dynamics-forced (AMV-DF) components in the partially and fully coupled simulations. The AMV, AMV-SF, and AMV-DF indices are computed respectively as the spatially averaged and low pass-filtered (10-year running mean) North Atlantic SSTs and its surface-forced and dynamics-forced components (i.e., surface values

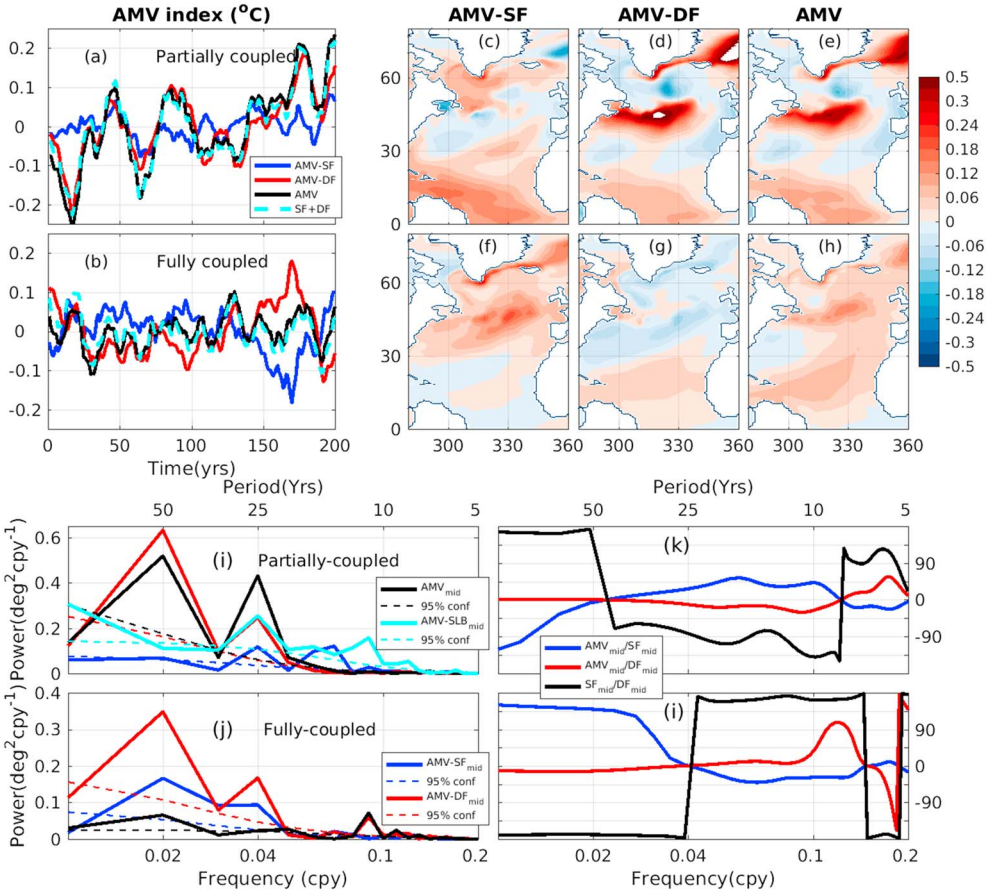

Figure 2. AMV index and its SF and DF components and their sum in the partially coupled (a) and fully coupled (b) simulations. AMV-SF, AMV-DF, and AMV patterns (partially coupled [c–e]; fully coupled [f–h]); power spectra of the AMV_{mid} index and its SF and DF components (slab/partially coupled [i]; fully coupled [j]); Partially coupled AMV-SF (blue line in i) is magnified 5X; dashed lines show 95% significance level of the corresponding autoregressive model. Phase relationship (degrees) between the AMV and its components and between the component (partially coupled [k]; fully coupled [l]). AMV = Atlantic multidecadal variability; DF = dynamics forced; SF = surface forced; THF = turbulent heat fluxes.

of T', T'_{AF}, and T'_{RF}; T'_{P}, T'_{AP}, and T'_{RP}, over 0° N to 60° N and 0–80° W). To remove any externally forced signal, the time series of their respective global surface averages are also subtracted from the indices, following Trenberth and Shea (2006). Their corresponding patterns are computed by regressing surface T' on the standardized AMV, AMV-SF, and AMV-DF indices.

Comparing the AMV index with the sum of its components indices attests to the accuracy of the decomposition (Figures 2a and 2b, black and cyan lines). In both simulations, the AMV index is often the same sign and in phase with its DF component, especially in the partially coupled simulation, suggesting the DF component is dominant (Figures 2a and 2b, black and red lines). The partially coupled AMV pattern is likewise similar to its DF pattern, while the fully coupled AMV is not similar to either of its components (compare Figures 2c, 2d and 2e and Figures 2f, 2g and 2h). It is noteworthy, however, that when the spatially averaged indices without low pass filtering are used to compute the patterns, the SF patterns are much more similar to the fully coupled AMV pattern, much like the similarity found in slab and fully coupled AMV patterns (compare Figures S1 and S2).

To see their relationship quantitatively, we examine the power spectra of the AMV_{mid} index and its components ($AMV\text{-}SF_{mid}$ and $AMV\text{-}DF_{mid}$), defined only over the midlatitude Atlantic region (40° N to 60° N and 0–80° W), in both simulations. The AMV_{mid} index is often used to study the dynamics of the AMV because of its stronger decadal to low-frequency power compared to the more damped AMV index (Gulev et al., 2013; O'Reilly et al., 2016; Zhang et al., 2016; compare Figures S3 and 2j). Nevertheless, the AMV_{mid} index is highly

correlated with the AMV index ($r = 0.7$), and the conclusions we show are not impacted qualitatively by the choice of index.

The fully coupled AMV_{mid} index shows significant low-frequency spectral power at 25- and 50-year periods (Figure 2j), capturing the 20- to 30-year and 50- to 80-year timescales found in observational studies and historical simulations (Delworth & Greatbatch, 2000; Frankcombe et al., 2010; Gulev et al., 2013; Zhang & Wang, 2013). However, this fully coupled AMV_{mid} spectrum is much weaker than the partially coupled AMV_{mid} spectrum (without ocean feedback), with only one tenth of the spectral power of the partially coupled AMV_{mid} at the 50-year period (Figures 2i and 2j, black lines). The greater low-frequency power of the partially coupled AMV_{mid} index is due to the much larger power of its DF component; its SF component is much weaker in comparison, though significant (Figure 2i, red; blue [magnified 5X] lines). In contrast, the much weaker fully coupled AMV_{mid} is due to the different spectral power and phase relationship of its components. The fully coupled DF spectrum, though similar to the partially coupled one, has about half the power at the 50-year period (Figure 2i and 2j, red lines), while the fully coupled SF spectrum is much stronger than the partially coupled SF spectrum at low frequencies (Figures 2i and 2j, blue lines) . Unlike the partially coupled components, the fully-coupled components are also totally out of phase with each other at all timescales (Figure 2k and 2l, black lines), so that the already reduced fully coupled DF component is also damped by a strong SF component, thereby causing the much reduced fully coupled AMV.

This analysis of the AMV components in the partially and fully coupled simulations suggests that fully coupled AMV is predominantly driven by ocean circulation variability. In both simulations, the significant low-frequency power of the AMV evidently arises because the spectral power of the ocean-forced components are greater than those of the surface-forced components. This is true even in the fully coupled simulation where the ocean-forced component is weaker, and damped by a strong surface-forced component. When decoupled from the atmosphere, the ocean-forced component has even greater power (partially coupled AMV-DF), indicating that the ocean is the source of this low-frequency variability.

Furthermore, the spectra change of surface-forced component between the two simulations also indicates that the fully coupled surface heat fluxes are largely ocean driven. The partially coupled AMV-SF variability, driven by surface heat fluxes which are decoupled from the ocean-forced SST anomalies (i.e., atmosphere-forced only), is weak and barely significant at low frequencies (Note that the partially coupled AMV-SF spectrum is also weaker than that of the slab AMV which is also atmosphere-forced, because of the lack of the realistic ocean damping in the slab model). However, the fully coupled AMV-SF spectrum is stronger (10 times the partially coupled AMV-SF) and even bears the imprint of the DF spectrum, because of the impact of the ocean-forced SST in fully coupled surface heat fluxes. Furthermore, unlike the partially coupled SF component, the fully coupled one is completely out of phase with its DF component because the fully coupled surface heat fluxes are largely damping ocean-forced SSTs; as a result, the fully-coupled SF anomalies which are the passive temperature response to these surface heat fluxes, are opposite in sign to the ocean-forced ones.

This analysis, therefore, suggests that the much weaker low-frequency power of the fully coupled AMV is not due to the absence of a strong ocean-forced variability, rather it results from the strength of coupling between the atmosphere and the ocean or the surface damping rate (λ_A), which damps the ocean-forced variability.

3.2. Surface Interaction of Components and Timescale Separation

To further understand how the AMV components interact at the surface, we compare their correlation and phase relationship with surface heat fluxes in the partially and fully coupled simulations. The spectra of the radiative and turbulent components of the surface heat fluxes indicate that the turbulent component, rather than the radiative component, is responsible for the ocean feedback in the fully coupled SF component; turbulent heat fluxes (THF) show much greater spectral power than the radiative fluxes, and the spectral change of these flux components between the simulations is only evident in the THF spectrum (Figures 3a and 3b, red lines). Therefore, we will focus on the correlation and phase relationship between the THF and the AMV index and its components in the following analysis.

To facilitate comparison with previous studies, we reverse the sign of the surface heat fluxes (into the ocean becomes negative) for this analysis. Therefore, a negative correlation or out-of-phase relationship with the THF (i.e., THFs into [out of] the ocean cause warm [cool] temperature anomalies) would indicate surface heat flux-driven temperature anomalies and vice versa. In both simulations, both AMV components show significant but opposite-signed correlations with the THF. As we would expect of the ocean passive temperature response to surface heat fluxes, the SF-THF correlation is negative, while the DF-THF correlation is positive

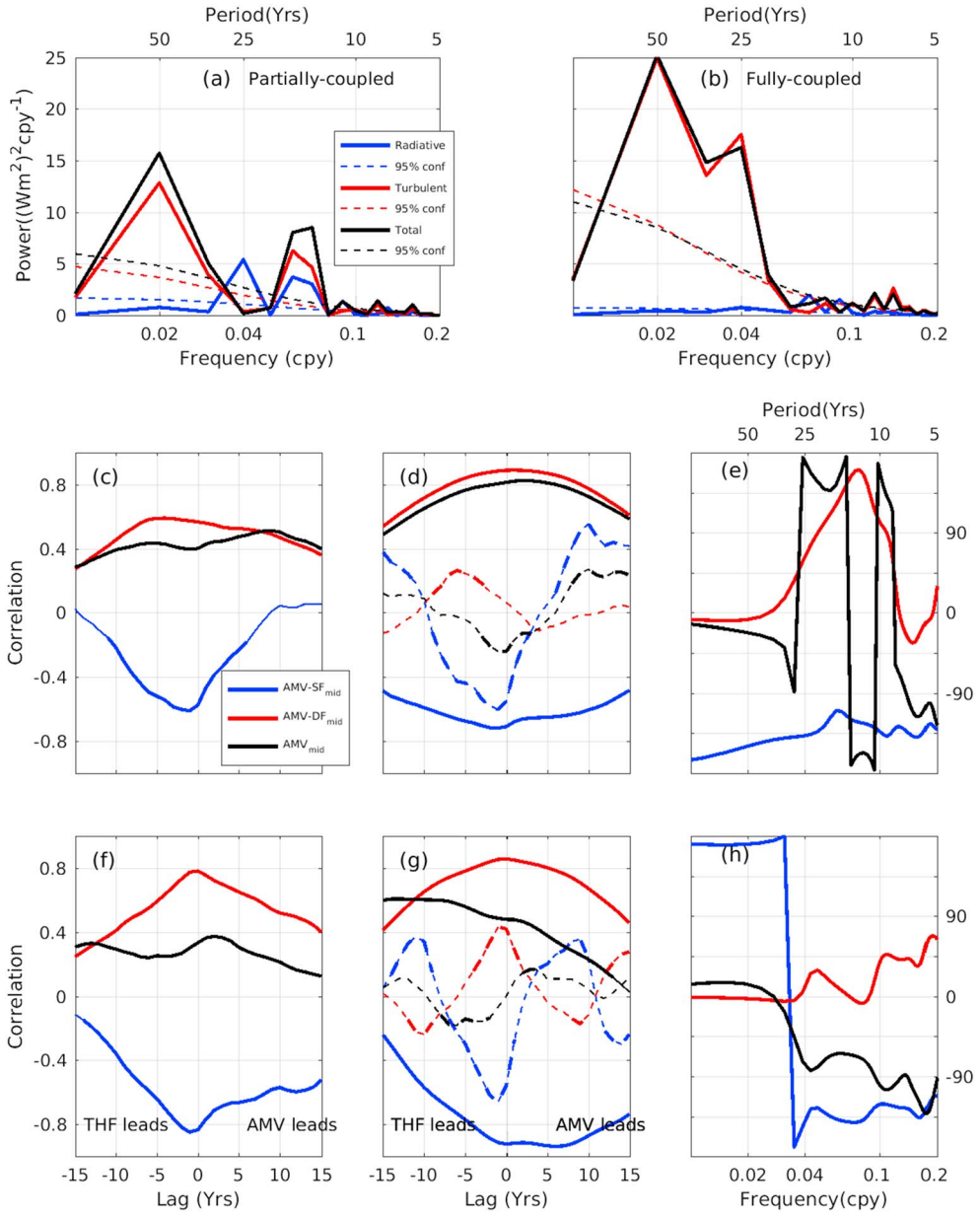

Figure 3. Power spectra of the spatially averaged midlatitude Atlantic (40° −60° N) total, radiative, and turbulent heat fluxes (THF) inidices (partially coupled [a]; fully coupled [b]). Radiative component is magnified 5X to show relative strength. Dashed lines indicate 95% significance level of the spectra. Correlation of the midlatitude Atlantic THF index with the AMV_{mid} index and its surface-forced and dynamics-forced components (partially coupled [c and d], fully coupled [f and g]). Correlation using 10-year moving average filtered indices (c and f). Thirty-year moving averaged filtered indices (d and g, solid lines); 10- to 30-year filtered indices: residual of the 10- and 30-year indices (d and g, dashed lines). Significant correlation values based on the Fisher test are shown in thick lines, while thin lines show insignificant values. Phase relationship between AMV_{mid} index, its respective components, and the THF (partially coupled [e], fully coupled [h]). AMV = Atlantic multidecadal variability; DF = dynamics forced; SF = surface forced; THF = turbulent heat fluxes.

(Figures 3c and 3f, red and blue lines). In the partially coupled simulation (where the DF component is not coupled), the positive DF-THF correlation suggests that surface heat fluxes are related to the circulation changes driving DF anomalies, while in the fully coupled case, it indicates that DF anomalies drive surface heat fluxes.

Nevertheless, in both simulations the AMV-THF correlation takes on the positive sign of the DF-THF correlation. It can be shown that the AMV-THF correlation is the variance-weighted sum of the correlations of the AMV

components with the THF (see Appendix A). Given the similar magnitude but opposite-signed correlations of its components, the AMV-THF correlation sign indicates the component with the greater proportion of the variance; else, it would have vanished if the opposite-signed components had similar variances. Thus, the positive AMV-THF correlation is consistent with the greater contribution of the DF component variance to the AMV spectra in both simulations (compare Figures 2i and 2j). Similarly, the negative SF-THF correlation in the fully coupled simulation is weighted more, because of the greater proportion of variance of the fully coupled SF component. As a result, the positive DF-THF correlation in the fully coupled simulation, though greater than the partially coupled one, is less dominant, causing the weaker positive AMV-THF correlation in this simulation (compare black lines in Figures 3c and 3f and Figures 3d and 3g).

To further examine the surface interaction of the components across timescales, we decompose the AMV-THF correlation into the interdecadal (10- 30-year periods) and multidecadal (>30-year periods) timescales (Figures 3d and 3g), based on the spectra peaks of the AMV and the components. It is evident that the ocean-driven AMV mechanism operates mainly on multidecadal timescales, at least in the model examined here; in both simulations, the positive DF-THF correlation is greater and dominant in the AMV-THF correlation at this timescale (compare solid and dashed lines in Figures 3d and 3g). In contrast, on interdecadal timescales, at most time lags, the DF-THF correlation is neither significant nor dominant in the AMV-THF correlation in both simulations; the DF-THF correlation is only significant when the AMV-THF correlation is not significant and THF leads. The SF-THF correlation is more dominant instead, indicating the atmosphere drives the AMV more at this timescale.

Furthermore, the lead-lag correlation pattern of the SF component, which is directly forced by the THF, suggests that different mechanisms operate on these different timescales. On multidecadal timescales, compared to the partially coupled simulation, the fully coupled SF-THF correlation decreases at THF lead times but increases at SF lead times (Figures 3d and 3g, solid blue lines). This SF-THF lead-lag correlation pattern change suggests that the fully coupled surface heat fluxes are primarily ocean-driven at this timescale. The weaker (stronger) correlation at the THF (SF) lead times suggests weaker atmosphere-driven than ocean-driven THF anomalies, especially because this correlation pattern appears when the surface heat fluxes are impacted by the DF component in the fully coupled simulation.

On interdecadal timescales, the SF-THF lead-lag correlation pattern suggests a passive ocean temperature response to atmosphere-driven surface heat fluxes. In both simulations, the SF-THF correlation is largely negative at THF lead times (max at 1-year lead) but largely positive at SF lead times (max at 10-year lead; Figure 3d and 3g, dashed blue lines). The negative correlation at the THF lead time indicate the warm (cool) ocean passive temperature response that surface heat fluxes into (out of) the ocean cause within a short time. The positive correlation at the longer SF lead time suggests that these warm (cool) passive anomalies later drive surface heat fluxes out (into) the ocean. This change is due to the larger heat capacity of the ocean, which causes ocean anomalies to persist, such that the ocean is eventually warmer (cooler) than the atmosphere and thus could drive surface heat fluxes. That this correlation pattern is clearer (and dominates the AMV-THF correlation) in the partially coupled simulation (i.e., without ocean feedback) further suggests that it is atmosphere driven.

The phase relationship between the THF and AMV or its components gives further evidence that different mechanisms operate on these timescales (Figure 3e and 3h). On multidecadal timescales, the AMV and its DF component are in phase with the THF (i.e., THF out of [into] the ocean is related to positive [negative] DF anomaly) in both simulations, indicating that the ocean drives the AMV at this timescale, not surface heat fluxes. On interdecadal timescales, the AMV and both of its components are out of phase with the THF indicating that surface heat fluxes or the atmosphere drive the AMV at this timescale. In the fully coupled simulation, this out-phase AMV-THF relationship is weaker; however, the AMV-THF phase is the same sign as that of SF-THF indicating the dominance of the SF-THF mechanism.

It is also noteworthy that the SST-THF correlation pattern in slab models (Figure S4) or noise-forced models, on timescales longer than 10 years shown in O'Reilly et al. (2016) and Cane et al. (2017), are also very similar to the atmosphere-driven interdecadal SF-THF correlation explained above. The slab AMV spectrum here also shows significant variability up to the interdecadal timescales (Figure 2i, cyan line). The decomposition here therefore suggests that the atmosphere-driven AMV mechanism of the slab model, though much weaker (due to damping by the ocean circulation, that is, $\vec{v}T'$), is also present in the fully coupled simulation on interdecadal timescales, at least in the model examined here. In the fully coupled simulation,

this atmosphere-driven variability is further overshadowed by a stronger ocean-driven variability on multidecadal timescales. The frequency ranges of the ocean-driven and atmosphere-driven mechanisms shown here should vary with different models.

4. Discussion and Summary

We examined the relative roles of the ocean and atmosphere in driving the AMV by decomposing North Atlantic SST variability into components driven by the surface heat flux (SF) and ocean dynamics variability (DF), in fully and partially coupled simulations. In the partially coupled simulation, the ocean-forced SST (DF) anomaly is prevented from interacting with the atmosphere, allowing us to isolate the purely atmosphere-driven surface heat fluxes and ocean temperature anomalies. We find that the variability driven by the ocean circulation is the dominant factor in determining the AMV spectra and its correlation with surface THF in both simulations. In the partially coupled simulation, surface heat fluxes due to atmospheric forcing alone (i.e., without the impact of the ocean-forced SST), drive weak SST variability up to interdecadal timescales, while ocean circulation drives a stronger variability on multidecadal timescales. Due to interaction with the atmosphere, the ocean-driven variability in the fully coupled simulation, though it still has greater multidecadal power than the atmosphere-driven variability, is weaker and also damped by surface heat fluxes—as a result, the fully coupled AMV power is much reduced.

One major implication of this decomposition is that the low-frequency power of the AMV simulated by models is influenced by the surface heat flux feedback or damping rate in the models. Despite the large multidecadal power of the ocean-forced component decomposed here, the fully coupled AMV power is much weaker due the damping of this ocean-forced variability by surface heat fluxes, which is in turn modulated by the surface damping rate in a model. Similarly, the positive AMV-THF correlation that comes from the dominant positive correlation of its ocean-forced component with the THF reduces in the fully coupled simulation compared to the partially coupled one because of the increase in the variance surface-forced component, which has a negative correlation with the THF. This increase is in the fully coupled SF variance is also due to the surface damping rate in the model. Fully coupled models generally simulate weaker AMV variability and a less positive AMV-THF correlation than observations (Gulev et al., 2013; O'Reilly et al., 2016); together, these indicate that the strength of the surface coupling in fully coupled models may often be too strong. The simulated AMV power depends on relative magnitudes of the surface- and ocean-forced components, which depend on other factors influencing ocean circulation variability (such as the ocean damping rate or mixed layer depth) or resolution; therefore, it would be useful to repeat this decomposition in other models.

The dominant ocean-forced component of the AMV decomposed here is consistent with the ocean-driven AMV mechanism demonstrated in earlier studies showing that surface heat fluxes damp rather than force SST anomalies at low frequencies (Gulev et al., 2013; O'Reilly et al., 2016; Zhang et al., 2016; Zhang, 2017). Compared to the ocean heat convergence diagnosed from fully coupled models, which has a flat spectra (Cane et al., 2017; Clement et al., 2015), the ocean-forced component here has large multidecadal power. This is because the ocean heat convergence is a function of both ocean-forced and surface-forced terms that are out of phase, thereby masks the large ocean-driven multidecadal variability and thus can be misleading.

Our analysis further provides some insight into the reason fully coupled and slab ocean models may produce similar AMV spectra, despite being ocean- and atmosphere-driven, respectively. The fully coupled AMV spectra is the residual of a large ocean-driven variability damped by surface heat fluxes, while the slab AMV is due to weak atmospheric forcing that only operates up to interdecadal timescales. The comparison of the slab AMV spectra and that of the partially coupled AMV-SF, which is also atmosphere driven, shows that the lack of a realistic ocean damping also enhances the slab AMV spectra (Zhang, 2017), such that slab AMV even has greater spectral power than the fully coupled AMV and the partially coupled AMV-SF.

Finally, we point out that the results here do not rule out that atmospheric noise may drive oceanic multidecadal variability, as demonstrated by interactive ensemble experiments (Chen et al., 2016; Fan & Schneider, 2012; Schneider & Fan, 2012). We have yet to examine the mechanisms behind the strong ocean-forced multidecadal variability. For instance, why is there a significant correlation between the atmosphere-forced surface heat fluxes and the ocean-forced temperature in the partially coupled experiment, despite being decoupled from each other by design? What roles do momentum and fresh water fluxes play in driving the ocean-forced component, and why does the ocean circulation-driven variability weaken in the fully coupled simulation? And what are the relative roles of the Atlantic meridional overturning circulation and subpolar gyre

circulation in driving the ocean-forced variability? Despite these unanswered questions, we have shown that ocean circulation variability is the dominant driver of the AMV and that air-sea coupling determines the power of the AMV in fully coupled models.

Appendix A: Correlation Decomposition

Let $X = X_1 + X_2$, $\sigma_{X_1} = P_1\sigma_X$, and $\sigma_{X_2} = P_2\sigma_X$.

σ_X is the standard deviation of X; σ_{X_1}, P_1 and σ_{X_2}, P_2 are standard deviations and the fraction of variance of the components X_1 and X_2, respectively.

Then the correlation between Y and X is given as

$$\rho(Y,X) = \frac{cov(Y,X)}{\sigma_Y\sigma_X}, \tag{A1}$$

where $cov(Y,X)$ is the covariance between Y and X

$$\rho(Y,X) = \frac{cov(Y,X_1)}{\sigma_Y\sigma_X} + \frac{cov(Y,X_2)}{\sigma_Y\sigma_X}, \tag{A2}$$

$$\rho(Y,X) = \frac{\rho(Y,X_1)\sigma_Y\sigma_{X_1}}{\sigma_Y\sigma_X} + \frac{\rho(Y,X_2)\sigma_Y\sigma_{X_2}}{\sigma_Y\sigma_X}. \tag{A3}$$

Using $\sigma_{X_1} = P_1\sigma_X$ and $\sigma_{X_2} = P_2\sigma_X$, we have

$$\rho(Y,X) = P_1\rho(Y,X_1) + P_2\rho(Y,X_2). \tag{A4}$$

Acknowledgments
This study is supported by the U.S. Department of Energy Office of Science and Biological and Environmental Research (BER) as part of the Regional and Global Climate Modeling Program. PNNL is operated for DOE by Battelle Memorial Institute under contract DE-AC05-76RL01830. H. A. S. is grateful for funding support from the Linus Pauling Distinguished Postdoctoral Fellowship at PNNL. F. L. is supported by the China Scholarship Council. Supercomputing resources are provided by National Energy Research Scientific Computing Center, a DOE Office of Science User Facility supported by the Office of Science of the U.S. Department of Energy under contract DE-AC02-05CH11231. The data set used for this work is available at http://doi.org/10.5281/zenodo.1134360. We thank the three anonymous reviewers for their helpful suggestions.

References

Banks, H. T., & Gregory, J. M. (2006). Mechanisms of ocean heat uptake in a coupled climate model and the implications for tracer based predictions of ocean heat uptake. *Geophysical Research Letters*, *33*, L07608. https://doi.org/10.1029/2005GL025352

Barsugli, J. J., & Battisti, D. S. (1998). The basic effects of atmosphere—Ocean thermal coupling on midlatitude variability. *Journal of the Atmospheric Sciences*, *55*(4), 477–493.

Bitz, C. M., Shell, K., Gent, P., Bailey, D., Danabasoglu, G., Armour, K., et al. (2012). Climate sensitivity of the community climate system model, version 4. *Journal of Climate*, *25*(9), 3053–3070.

Bouttes, N., Gregory, J., Kuhlbrodt, T., & Smith, R. (2014). The drivers of projected north Atlantic sea level change. *Climate Dynamics*, *43*(5-6), 1531–1544.

Cane, M. A., Clement, A. C., Murphy, L. N., & Bellomo, K. (2017). Low-pass filtering, heat flux and Atlantic multidecadal variability. *Journal of Climate*, *30*, 7529–7553.

Chen, H., Schneider, E. K., & Wu, Z. (2016). Mechanisms of internally generated decadal-to-multidecadal variability of SST in the Atlantic Ocean in a coupled GCM. *Climate Dynamics*, *46*(5-6), 1517–1546.

Clement, A., Bellomo, K., Murphy, L. N., Cane, M. A., Mauritsen, T., Rädel, G., & Stevens, B. (2015). The Atlantic multidecadal oscillation without a role for ocean circulation. *Science*, *350*(6258), 320–324.

Clement, A., Cane, M. A., Murphy, L. N., Bellomo, K., Mauritsen, T., & Stevens, B. (2016). Response to comment on "The Atlantic multidecadal oscillation without a role for ocean circulation". *Science*, *352*(6293), 1527–1527. https://doi.org/10.1126/science.aaf2575

Danabasoglu, G., Bates, S. C., Briegleb, B. P., Jayne, S. R., Jochum, M., Large, W. G., et al. (2012). The CCSM4 ocean component. *Journal of Climate*, *25*(5), 1361–1389.

Delworth, T. L., & Greatbatch, R. J. (2000). Multidecadal thermohaline circulation variability driven by atmospheric surface flux forcing. *Journal of Climate*, *13*(9), 1481–1495.

Fan, M., & Schneider, E. K. (2012). Observed decadal north Atlantic tripole SST variability. Part I: Weather noise forcing and coupled response. *Journal of the Atmospheric Sciences*, *69*(1), 35–50.

Frankcombe, L. M., Von Der Heydt, A., & Dijkstra, H. A. (2010). North Atlantic multidecadal climate variability: An investigation of dominant time scales and processes. *Journal of Climate*, *23*(13), 3626–3638.

Frankignoul, C. (1985). Sea surface temperature anomalies, planetary waves, and air-sea feedback in the middle latitudes. *Reviews of Geophysics*, *23*(4), 357–390. https://doi.org/10.1029/RG023i004p00357

Frankignoul, C., Kestenare, E., & Mignot, J. (2002). The surface heat flux feedback. Part II: Direct and indirect estimates in the ECHAM4/OPA8 coupled GCM. *Climate Dynamics*, *19*(8), 649–655.

Garuba, O. A., & Klinger, B. (2016). Ocean heat uptake and interbasin transport of the passive and redistributive components of surface heating. *Journal of Climate*, *29*(20), 7507–7527. https://doi.org/10.1175/JCLI-D-16-0138.1

Garuba, O. A., Lu, J., Liu, F., & Singh, H. A. (2018). The active role of the ocean in the temporal evolution of climate sensitivity. *Geophysical Research Letters*, *45*, 306–315. https://doi.org/10.1002/2017GL075633

Goodman, J., & Marshall, J. (1999). A model of decadal middle-latitude atmosphere—Ocean coupled modes. *Journal of Climate*, *12*(2), 621–641.

Gregory, J. M., Bouttes, N., Griffies, S. M., Haak, H., Hurlin, W. J., Jungclaus, J., et al. (2016). The Flux-Anomaly-Forced Model Intercomparison Project (FAFMIP) contribution to CMIP6: Investigation of sea-level and ocean climate change in response to CO_2 forcing. *Geoscientific Model Development*, *9*(11), 3993–4017. https://doi.org/10.5194/gmd-9-3993-2016

Gulev, S. K., Latif, M., Keenlyside, N., Park, W., & Koltermann, K. P. (2013). North Atlantic Ocean control on surface heat flux on multidecadal timescales. *Nature*, *499*(7459), 464–467.

Hunke, E. C., Lipscomb, W. H., Turner, A. K., Jeffery, N., & Elliott, S. (2010). CICE: The Los Alamos sea ice model documentation and software user's manual version 4.1 (*LA-CC-06-012*). Los Alamos: T-3 Fluid Dynamics Group, Los Alamos National Laboratory. 675.

Knight, J. R., Allan, R. J., Folland, C. K., Vellinga, M., & Mann, M. E. (2005). A signature of persistent natural thermohaline circulation cycles in observed climate. *Geophysical Research Letters*, *32*, L20708. https://doi.org/10.1029/2005GL024233

Kushnir, Y. (1994). Interdecadal variations in North Atlantic sea surface temperature and associated atmospheric conditions. *Journal of Climate*, *7*(1), 141–157.

Marshall, J., Scott, J. R., Armour, K. C., Campin, J. M., Kelley, M., & Romanou, A. (2015). Ocean's role in the transient response of the climate to abrupt greenhouse gas forcing. *Climate Dynamics*, *44*(7-8), 2287–2299.

Msadek, R., & Frankignoul, C. (2009). Atlantic multidecadal oceanic variability and its influence on the atmosphere in a climate model. *Climate Dynamics*, *33*(1), 45–62.

Neale, R. B., Chen, C.-C., Gettelman, A., Lauritzen, P. H., Park, S., Williamson, D. L., et al. (2010). Description of the NCAR Community Atmosphere Model (CAM 5.0) (NCAR Technical Note NCAR/TN-486+ STR). Boulder, CO: National Center for Atmospheric Research.

O'Reilly, C. H., Huber, M., Woollings, T., & Zanna, L. (2016). The signature of low-frequency oceanic forcing in the Atlantic multidecadal oscillation. *Geophysical Research Letters*, *43*, 2810–2818. https://doi.org/10.1002/2016GL067925

Oleson, K. W., Lawrence, D. M., Gordon, B., Flanner, M. G., Kluzek, E., Peter, J., et al. (2010). Technical description of version 4.0 of the Community Land Model (CLM) (NCAR Technical Note NCAR/TN-478+STR). Boulder, CO: National Center for Atmospheric Research.

Schneider, E. K., & Fan, M. (2012). Observed decadal North Atlantic tripole SST variability. Part II: Diagnosis of mechanisms. *Journal of the Atmospheric Sciences*, *69*(1), 51–64.

Singh, H. K., Hakim, G. J., Tardif, R., Emile-Geay, J., & Noone, D. C. (2018). Insights into Atlantic multidecadal variability using the Last Millennium Reanalysis framework. *Climate of the Past*, *14*(2), 157–174.

Srivastava, A., & DelSole, T. (2017). Decadal predictability without ocean dynamics. *Proceedings of the National Academy of Sciences*, *114*(9), 2177–2182.

Trenberth, K. E., & Shea, D. J. (2006). Atlantic hurricanes and natural variability in 2005. *Geophysical Research Letters*, *33*, L12704. https://doi.org/10.1029/2006GL026894

Xie, P., & Vallis, G. K. (2012). The passive and active nature of ocean heat uptake in idealized climate change experiments. *Climate Dynamics*, *38*(3-4), 667–684. https://doi.org/10.1007/s00382-011-1063-8

Zhang, R. (2017). On the persistence and coherence of subpolar sea surface temperature and salinity anomalies associated with the Atlantic multidecadal variability. *Geophysical Research Letters*, *44*, 7865–7875. https://doi.org/10.1002/2017GL074342

Zhang, R., Sutton, R., Danabasoglu, G., Delworth, T. L., Kim, W. M., Robson, J., & Yeager, S. G. (2016). Comment on "The Atlantic multidecadal oscillation without a role for ocean circulation". *Science*, *352*(6293), 1527–1527.

Zhang, L., & Wang, C. (2013). Multidecadal North Atlantic sea surface temperature and Atlantic meridional overturning circulation variability in CMIP5 historical simulations. *Journal of Geophysical Research: Oceans*, *118*, 5772–5791. https://doi.org/10.1002/jgrc.20390